TECHNICAL ARTICLE

Molecular reorientation in a dehydration process of an organic polar salt of 2,4-diaminotoluene/L(+)-tartaric acid

Weicai Ju, Simin Qiu, Yaqiu Tao, Xiaodong Shen, and Zhigang Pan[a)]
College of Materials Science and Engineering, Nanjing Tech University, No. 5 Xinmofan Road, Nanjing, China

(Received 25 February 2016; accepted 1 December 2016)

An organic polar hydrate was obtained through cocrystallization of 2,4-diaminotoluene (2,4-DAT) and L(+)-tartaric acid (TA) from ethanol. Dehydration behavior of the obtained hydrate was investigated using variable temperature powder X-ray diffraction (PXRD) and thermal analysis. Proton transfer from L(+)-TA to 2,4-DAT in both hydrate and dehydrated form was revealed via Fourier transform infrared spectroscopy. The crystal structures of both forms were determined using PXRD techniques. The similarities and differences between two crystal structures were analyzed and the role of water in the hydrate crystal structure was demonstrated. © *2017 International Centre for Diffraction Data*. [doi:10.1017/S0885715616000737]

Key words: organic polar materials, cocrystallization, dehydration

I. INTRODUCTION

Organic polar substances are potential functional materials, which have been attractive alternatives to their inorganic counterpart (Hu *et al.*, 2009). A great number of research activities have been focused on design and synthesis of organic polar materials and exploration of their potential ferroelectric properties (Chen, and Zeng, 2014). One design strategy is to introduce permanent dipoles to the desired materials, so that ferroelectric phenomenon arises from the orientation of these polar components (Tanase *et al.*, 2005; Fu *et al.*, 2013, 2011; Wen *et al.*, 2013). Alternatively, ferroelectricity can be achieved via displacement of ions in corresponding organic materials, such as charge–transfer complexes (Collet *et al.*, 2003; Chen & Zeng, 2014). As an analogy to charge–transfer complexes, cocrystals/salts based on acid and basic components are binary or multi-component systems in which the interactions among the molecules in the crystal structure are dominated by hydrogen bonding and not charge–transfer interactions (Katrusiak and Szafranski, 1999; Szafranski *et al.*, 2002; Horiuchi *et al.*, 2005).

Compounds containing carboxylic acid functional groups are excellent proton donors that can readily cocrystsallize with organic compounds containing nitrogen (Leiserowitz, 1976). Therefore, compounds with carboxylic acid functional groups are widely used in crystal engineering for cocrystals/salts with desired physical and chemical properties. Herein, L(+)-tartaric acid (TA) was chosen as a proton donor and 2,4-diaminotoluene (2,4-DAT) as a proton acceptor (Scheme 1). Several neutral cocrystals or ionic salts of TA with basic nitrogen-containing compounds have been crystallized and their crystal structures were deposited at the Cambridge Crystallographic Data Center (Aakeroy *et al.*, 1996; Timofeeva *et al.*, 2003; Smith *et al.*, 2006; Ding *et al.*, 2014).

In this contribution, an organic polar hydrate 2,4-DTA:TA:H_2O = 1:1:1 (**1**) and its dehydrated form (**2**) were synthesized. Powder X-ray diffraction (PXRD) techniques were employed to determine the crystal structures of **1** and **2**. Both **1** and **2** crystallized in the polar space group $P2_1$. Dehydration behavior was investigated using a combination of variable temperature PXRD, differential scanning calorimetry (DSC), thermogravimetric analysis (TGA), and Fourier transform infrared (FT-IR) spectroscopy.

II. EXPERIMENTAL

A. Preparation

All starting materials were purchased from Sinopharm Chemical Reagent Co., Ltd. and used without further purification. **1** was prepared by refluxing 1:1 stoichiometric quantities of 2, 4-DTA (110 mg, 0.9 mmol) and TA (135 mg, 0.9 mmol) in ethanol (10 ml). A suspension was obtained because of the limited solubility of TA in ethanol and therefore distilled water was added to the suspension dropwise under continuous stirring until the samples dissolved completely. The solution was then allowed to cool down to ambient temperature and a white precipitate was obtained after 24 h. **2** was obtained by heating **1** in the oven at 70 °C over a period of 5 h.

B. FT-IR characterization

FT-IR spectra were recorded on a Nicolet Nexus 670 series FT-IR spectrophotometer in an ATR mode. The spectra were measured under ambient conditions over the range 4000–650 cm^{-1} with a resolution of 4 cm^{-1}.

C. Powder X-ray diffraction

PXRD patterns were recorded on a Rigaku SmartLab 9 kW diffractometer equipped with a Cu$K_{\alpha 1}$ radiation (Ge-monochromated, λ = 1.54056 Å). For identification purposes, the samples were ground and loaded on a

[a)]Author to whom correspondence should be addressed. Electronic mail: panzhigang@njtech.edu.cn

https://doi.org/10.1017/S0885715616000737 Published online by Cambridge University Press

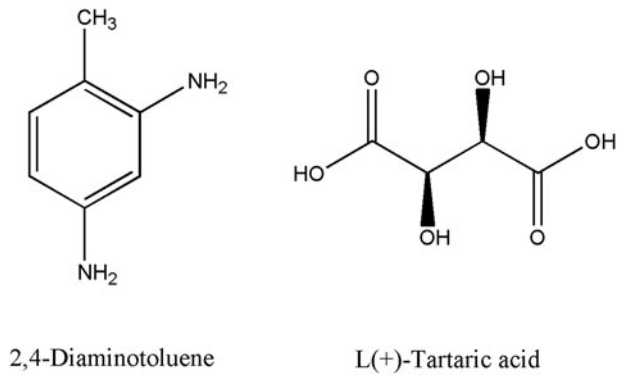

Scheme 1.

zero-background Si sample holder and PXRD data were collected in reflection mode in the 2θ range 5°–50° with a scan speed of 10° min^{-1}. For the measurement of PXRD data for structure determination, the samples were ground finely and loaded into borosilicate capillaries (0.7 mm diameter). High-quality PXRD data were acquired in transmission mode in the 2θ range 5°–70° with a scan speed of 0.5° min^{-1}. The capillary was spun at 20 rpm to improve powder averaging. Variable temperature PXRD experiment was carried out using the same diffractometer equipped with a high-temperature chamber (Anton Paar HTK 2000) and a TCU 2000N temperature control unit. The samples were loaded on a platinum plate and heated at 10 °C min^{-1}. Variable temperature PXRD patterns were recorded at different temperatures ranging from 30 to 140 °C in the range of 2θ = 5°–50° with a scan speed of 5° 2θ min^{-1}.

D. Thermal analysis

Thermal analysis was conducted using a NETSZCH STA449C Model DSC equipped with TA thermal analyzer. TGA/DSC experiment was carried out within a temperature range 30–200 °C at a heating rate of 2 °C min^{-1} under nitrogen atmosphere.

E. Crystal structure determination

For crystal structure determination of both **1** and **2**, the Materials Studio software package was employed for indexing and structure solution using the modules *X-CELL* (Neumann, 2003) and *PowderSolve* (Engel *et al.*, 1999), respectively. The space group was determined according to the systematic absences in combination with density considerations. Rietveld refinement was carried out using the *GSAS* (Larson, and Von Dreele, 2000) software package interfaced by *EXPGUI* (Toby, 2001). During Rietveld refinement, standard bond length and bond angle restraints ($d_{C–C,alkane}$ = 1.50 Å, $d_{C–C,aromatic}$ = 1.40 Å, $d_{C–O}$ = 1.36 Å, and $d_{C=O}$ = 1.21 Å) were applied to the TA and 2,4-DTA molecules. A planar restraint was applied to the aromatic ring in 2,4-DTA. Isotropic thermal displacement parameters were refined with a common value for each molecule. The restraints were gradually relaxed toward the end of Rietveld refinement. In the final stage of Rietveld refinement, hydrogen atoms were introduced based on the geometric considerations ($d_{C–H}$ = 0.95 Å, $d_{N–H}$ = 0.90 Å, and $d_{O–H}$ = 0.90 Å) using the *Crystals* software package (Betteridge *et al.*, 2003). It is important to note that no physical meaning should be assigned to the positions of H atoms since it is hard to locate hydrogen atoms unambiguously via laboratory PXRD techniques.

III. RESULTS AND DISCUSSION

A. Crystal structure of 1

The high-quality PXRD data of **1** were indexed on a primitive monoclinic unit cell with a = 7.56 Å, b = 16.41 Å, c = 5.33 Å, and β = 99.83°. Systematic absences are in consistent with the space groups $P2_1$ or $P2_1/m$. Density considerations indicate there are two TA and 2,4-DTA molecules in the unit cell and therefore the space group $P2_1$ was chosen for the subsequent structure solution. Initial structure solution using one TA and 2,4-DTA molecule in the asymmetric unit was reasonable in terms of the analysis of close contacts and hydrogen bonding interactions. However, the large difference between the calculated and experimental PXRD patterns indicated that the proposed structure was incomplete. A TGA/DSC analysis was then carried out (see Section 3.5) to find out whether water or other solvent molecules are present in the lattice. TGA suggested that there is one water molecule per TA and 2,4-DTA adduct. Therefore, the final structure solution was carried out using one TA molecule, one 2,4-DTA molecule, and one water molecule as the structural fragments in the asymmetric unit. During the structure solution stage, a total of 17 variables were allowed to optimize. A reasonable structure solution was obtained after two cycles of 150 000 simulated annealing steps and taken as the starting model for Rietveld refinement. Prior to Rietveld refinement, a Le Bail fit was carried out to determine the values of parameters relating to peak shape functions, zero point shift. A Le Bail fit also provides a criterion to evaluate the quality of final Rietveld refinement. The final refined unit-cell parameters are: a = 7.5721(1) Å, b = 16.3999(4) Å, c = 5.3316(1) Å, and β = 99.791(2)°. Final Rietveld refinement (R_{wp} = 9.33%, R_p = 7.26%, and χ^2 = 4.4) together with the Le Bail fit (R_{wp} = 8.14%, R_p = 6.28%, and χ^2 = 4.0) is shown in Figure 1. The fractional coordinates for non-hydrogen atoms of **1** are given in Table I.

In the crystal structure of **1**, each TA molecule is involved in hydrogen bonding with four neighboring TA molecules, three neighboring 2,4-DTA molecules, and two water molecules. As shown in Figure 2(a), all oxygen atoms in **1** participate in hydrogen bonding. In the 2,4-DAT molecule, the amino group at the 4-position forms hydrogen bonds with neighboring TA molecules, while the other amino group at the 2-position is involved in hydrogen bonding with the water molecule [Figure 2(b)]. Parallel chains of TA molecules and chains of a mixture of 2,4-DAT and water molecules are formed along the a-axis, resulting an alternative stacking of 2,4-DAT and TA molecules along the b-axis, as shown in Figure 3.

B. Variable temperature PXRD of 1

A variable temperature PXRD experiment was performed to understand the dehydration process of **1**. As shown in Figure 4, a gradual alteration of PXRD patterns was observed as the sample was heated from ambient temperature to 140 °C.

https://doi.org/10.1017/S0885715616000737 Published online by Cambridge University Press

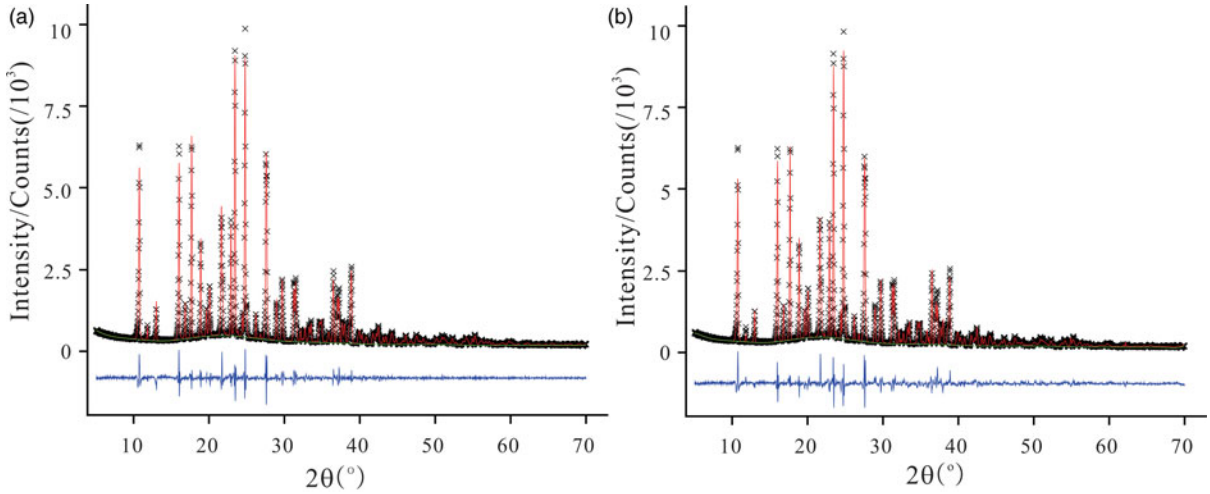

Figure 1. (Color online) Le Bail fit (a) and Rietveld refinement (b) of **1** showing the experimental pattern (solid red line), the simulated pattern (green crosses), and the difference between the simulated and experimental data (black lower line). Tick marks indicate the reflection positions.

TABLE I. Fractional coordinates of non-hydrogen atoms of **1**.

Atom	x	y	z	U_{iso}
C1	−0.1013 (2)	0.7546 (1)	0.4080 (5)	0.040 (1)
C2	0.0839 (1)	0.74442 (6)	0.3386 (2)	0.040 (1)
C3	0.1734 (1)	0.82674 (4)	0.3287 (2)	0.040 (1)
C4	0.3492 (4)	0.8184 (1)	0.2439 (6)	0.040 (1)
O5	−0.2423 (4)	0.7572 (5)	0.2330 (7)	0.040 (1)
O6	0.0725 (2)	0.70396 (7)	0.0990 (2)	0.040 (1)
O7	0.0592 (3)	0.88011 (4)	0.1599 (4)	0.040 (1)
O8	0.3755 (6)	0.8516 (5)	0.0522 (10)	0.040 (1)
O9	0.4782 (4)	0.7739 (5)	0.3824 (12)	0.040 (1)
O10	−0.1149 (3)	0.7695 (6)	0.6494 (7)	0.040 (1)
C15	0.5424 (1)	0.54801 (9)	0.5455 (3)	0.050 (2)
C16	0.5024 (1)	0.48340 (9)	0.3647 (3)	0.050 (2)
C17	0.33790 (5)	0.44280 (4)	0.3347 (1)	0.050 (2)
C18	0.2080 (1)	0.46644 (9)	0.4863 (3)	0.050 (2)
C19	0.2463 (1)	0.53008 (9)	0.6654 (3)	0.050 (2)
C20	0.41399 (5)	0.57141 (4)	0.6966 (1)	0.050 (2)
C21	0.45139 (2)	0.63899 (1)	0.88839 (3)	0.050 (2)
N22	0.7094 (1)	0.5869 (1)	0.5697 (4)	0.050 (2)
N23	0.29930 (2)	0.37729 (1)	0.15040 (3)	0.050 (2)
O30	−0.1115 (6)	0.5438 (6)	0.0900 (7)	0.102 (5)

The intensity of the reflection at around 13° increased gradually, while the reflection at around 22° shifted toward higher 2θ angles and a double reflection at around 28° became one single reflection. Dehydration of **1** completed at 130 °C.

C. Crystal structure of 2

The structure determination of **2** was carried out using the similar strategy to that for **1**. The final refined unit cell parameters are: $a = 7.5340(1)$ Å, $b = 16.1460(4)$ Å, $c = 5.3681(1)$ Å, and $\beta = 99.813(2)°$. Final Rietveld refinement ($R_{wp} = 8.80\%$, $R_p = 6.96\%$, and $\chi^2 = 5.3$) together with the Le Bail fit ($R_{wp} = 7.68\%$, $R_p = 5.91\%$, and $\chi^2 = 4.0$) is shown in Figure 5.

In the crystal structure of **2**, each TA molecule form hydrogen bonds with four neighboring TA and four neighboring 2,4-DAT molecules. All oxygen atoms except O(6) are involved in hydrogen bonding, as shown in Figure 6(a). The amino group at the 4-position of 2,4-DAT form hydrogen bonds with carboxylic groups from three neighboring TA molecules, while the other amino group at 2-poistion form a hydrogen bond with the hydroxyl group from one neighboring TA molecule, as shown in Figure 6(b). Parallel chains of TA molecules and parallel chains of the 2,4-DAT molecules are formed along the a-axis, leading to an alternative stacking of TA and 2,4-DAT along the b-axis shown in Figure 7. The fractional coordinates for non-hydrogen atoms of **2** are given in Table II.

D. Comparison of the crystal structures of 1 and 2

Crystal data, structural information and Rietveld refinement details of the crystal structure of **1** and **2** are summarized in Table III. When **1** was dehydrated to form **2**, the TA

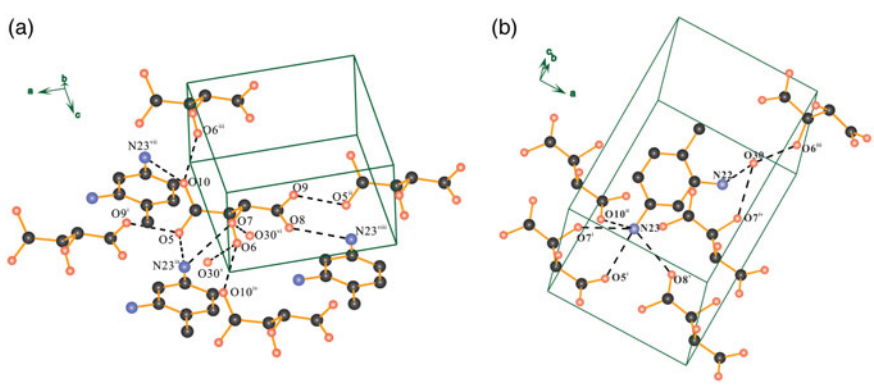

Figure 2. (Color online) Hydrogen bonding interactions around TA (a) and 2,4-DAT (b) in **1**. H atoms have been omitted for clarity. Carbon atoms are shown in dark gray, nitrogen in blue, and oxygen in red. Dashed lines represent hydrogen bonds. Symmetry code: (a) i $(1+x, y, z)$; ii $(-1+x, y, z)$; iii $(x, y, -1+z)$; iv $(x, y, 1+z)$; v (x, y, z); vi $(2-x, 0.5+y, 2-z)$; vii $(2-x, 0.5+y, 1-z)$; viii $(1-x, 0.5+y, 2-z)$; ix $(2-x, 0.5+y, 2-z)$. (b) i $(-x, -0.5+y, 1-z)$; ii $(-x, -0.5+y, 2-z)$; iii $(1+x, y, 1+z)$; iv $(1-x, -0.5+y, 2-z)$; v $(1-x, -0.5+y, 1-z)$.

https://doi.org/10.1017/S0885715616000737 Published online by Cambridge University Press

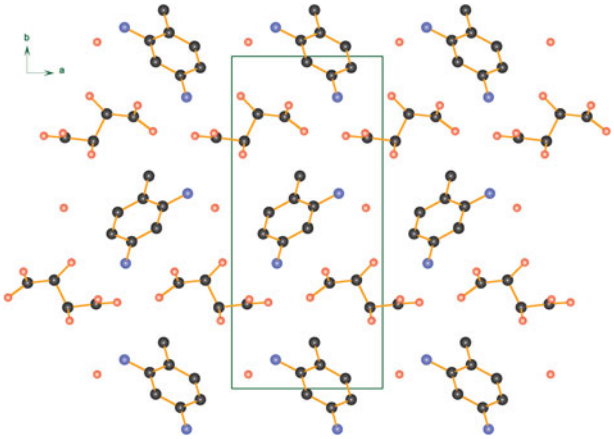

Figure 3. (Color online) Packing diagram of the crystal structure of **1** viewed along the *c*-axis, showing the 2,4-DAT and TA molecules arranged in separate stacks, which alternate along the *b*-axis. H atoms have been omitted for clarity. Color code is as in Figure 2.

molecules remain approximately the same position while 2,4-DAT molecules changed their orientations shown in Figure 8. As a result, the crystal structures of **1** and **2** share similarities in the arrangement of the TA molecules. In both crystal structures of **1** and **2**, as shown in Figure 9, parallel chains of TA molecules along the *a*-axis are formed via hydrogen bonds between carboxyl acid groups. On the other hand, the arrangements of the 2,4-DAT molecules are different. In the crystal structure of **1**, the 2,4-DAT molecules are linked to the TA molecular chains via hydrogen bonds involving the amino group at the 4-position. The water molecules in **1** form hydrogen bonds with hydroxyl groups from adjacent TA molecules. The water molecule also forms a hydrogen bond with the amino group at the 2-position. In the crystal structure of **2**, because of the loss of the water molecules, the TA and 2,4-DAT molecules are interlinked via hydrogen bonds involving the amino groups from the 2,4-DAT molecules and carboxylic/hydroxyl groups from TA molecules.

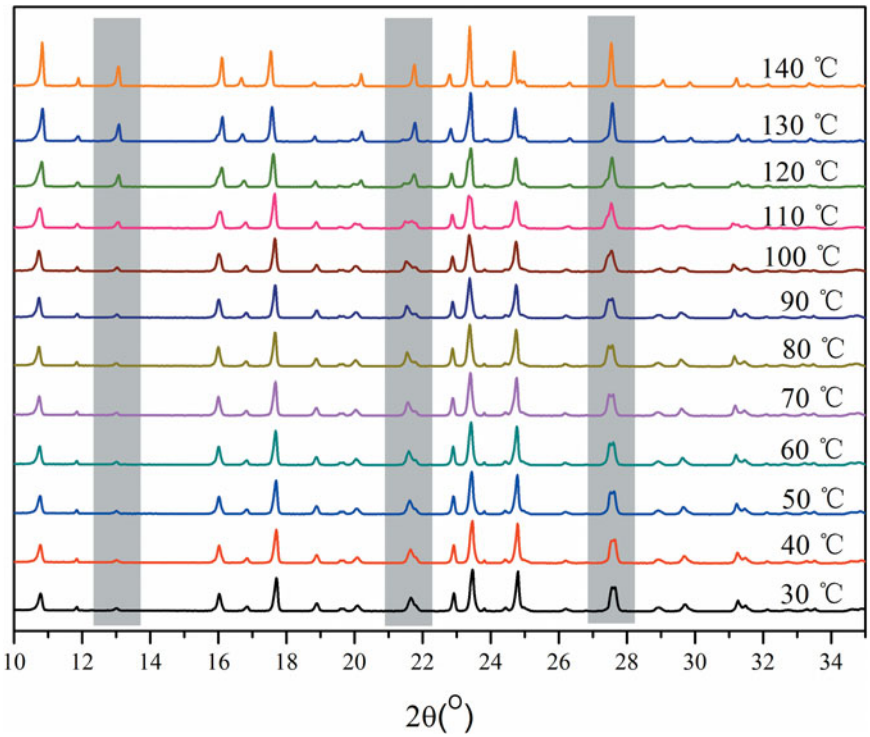

Figure 4. (Color online) Variable temperature PXRD patterns of **1**.

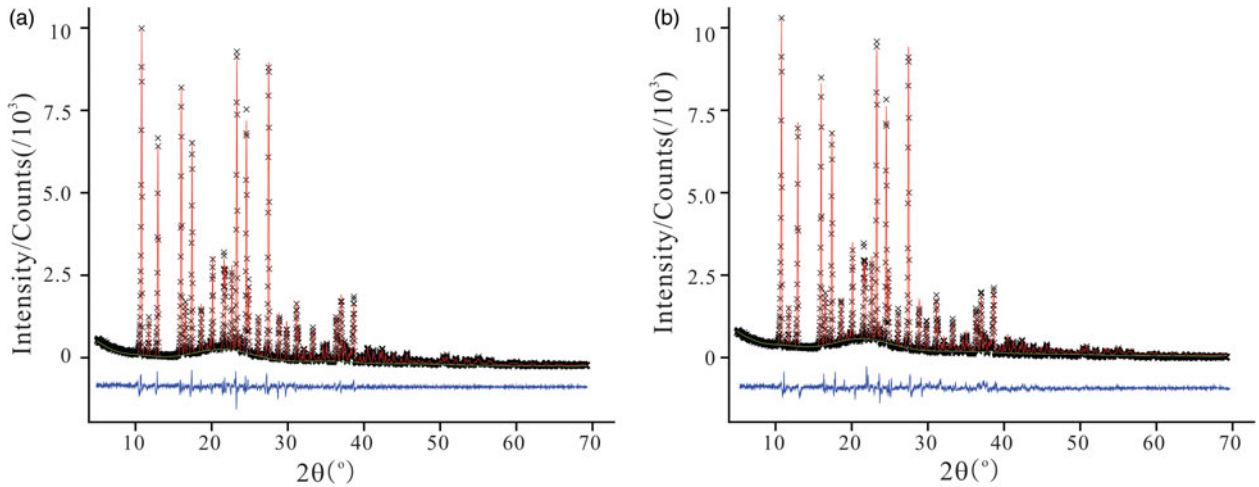

Figure 5. (Color online) Le Bail fit (a) and Rietveld refinement (b) of **2** showing the experimental pattern (solid red line), the simulated pattern (green crosses), and the difference between the simulated and experimental data (black lower line). Tick marks indicate the reflection positions.

https://doi.org/10.1017/S0885715616000737 Published online by Cambridge University Press

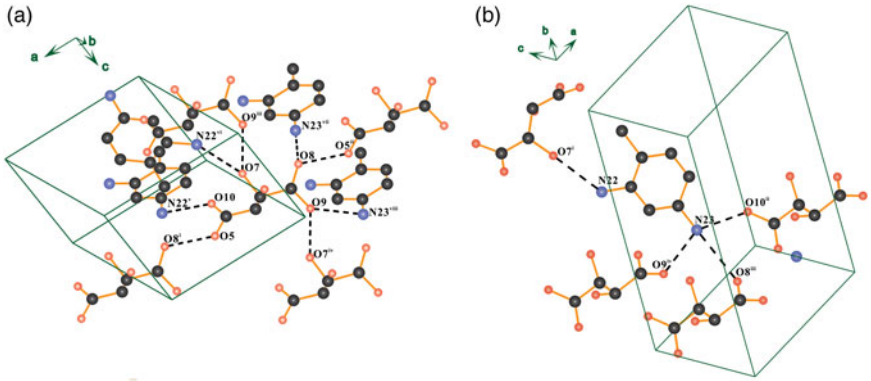

Figure 6. (Color online) Hydrogen bonding arrangements in **2**. Color code is as in Figure 2. Symmetry code: (a) i (1 + x, y, z); ii (−1 + x, y, z); iii (x, y, −1 + z); iv (x, y, 1 + z); v (1 + x, 0.5 + y, 1–z); vi (x, y, −1 + z); vii (−x, 0.5 + y, 1–z); viii (−x, 0.5 + y, 2–z). (b) i (x, y, 1 + z); ii (1–x, −0.5 + y, 1–z); iii (−x, −0.5 + y, 1−z); iv (−x, −0.5 + y, 2–z).

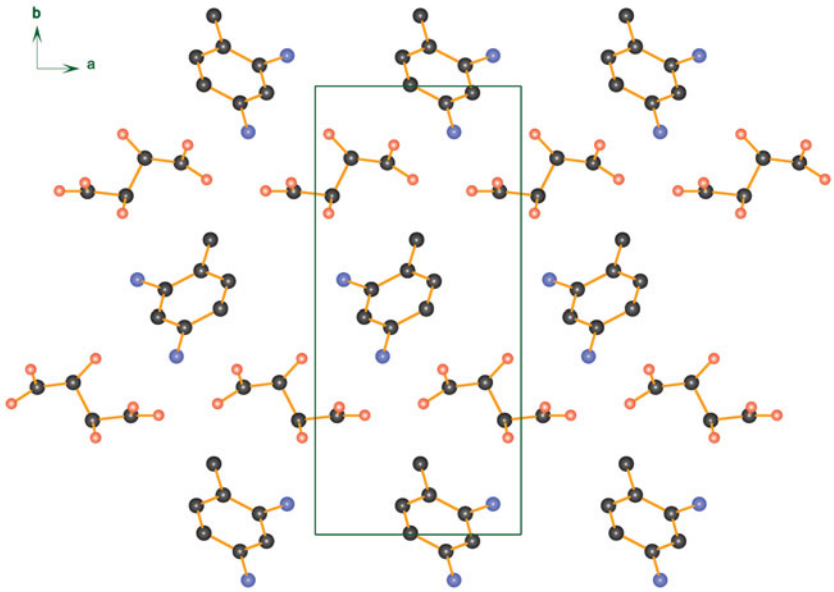

Figure 7. (Color online) Packing diagram of the crystal structure of **2** viewed along the *c*-axis, showing the 2,4-DAT and TA molecules arranged in separate stacks, which alternate along the *b*-axis. H atoms have been omitted for clarity.

TABLE II. Fractional coordinates of non-hydrogen atoms of **2**.

Atom	*x*	*y*	*z*	U_{iso}
C1	0.3479 (3)	0.8295 (1)	0.7631 (4)	0.033 (1)
C2	0.1738 (1)	0.83961 (9)	0.8427 (2)	0.033 (1)
C3	0.0807 (1)	0.7555 (1)	0.8490 (2)	0.033 (1)
C4	−0.1046 (2)	0.7652 (1)	0.9249 (6)	0.033 (1)
O5	0.4726 (4)	0.7922 (4)	0.9005 (9)	0.033 (1)
O6	0.0653 (1)	0.8933 (1)	0.6807 (5)	0.033 (1)
O7	0.0645 (3)	0.71621 (7)	0.6093 (2)	0.033 (1)
O8	−0.2395 (4)	0.7650 (6)	0.7638 (9)	0.033 (1)
O9	−0.1154 (5)	0.7855 (6)	1.1577 (9)	0.033 (1)
O10	0.3795 (6)	0.8692 (4)	0.5550 (9)	0.033 (1)
C15	0.2719 (1)	0.5468 (1)	1.1497 (3)	0.040 (1)
C16	0.2367 (1)	0.4855 (1)	0.9717 (3)	0.040 (1)
C17	0.36550 (6)	0.46240 (5)	0.8259 (1)	0.040 (1)
C18	0.5397 (1)	0.5037 (1)	0.8638 (3)	0.040 (1)
C19	0.5771 (1)	0.5646 (1)	1.0402 (3)	0.040 (1)
C20	0.44660 (6)	0.58869 (5)	1.1882 (1)	0.040 (1)
C21	0.49139 (3)	0.65759 (1)	1.3858 (4)	0.040 (1)
N22	0.1366 (1)	0.5682 (1)	1.2930 (4)	0.040 (1)
N23	0.32619 (2)	0.39820 (1)	0.6412 (4)	0.040 (1)

TABLE III. Crystal data and structure refinement for **1** and **2**.

	1	2
Formula	$(C_4H_6O_6)\cdot(C_7H_{10}N_2)\cdot H_2O$	$(C_4H_6O_6)\cdot(C_7H_{10}N_2)$
Formula weight	290.27	272.25
Crystal system	Monoclinic	Monoclinic
Space group	$P2_1$	$P2_1$
a (Å)	7.5721 (1)	7.5340 (1)
b (Å)	16.3999 (4)	16.1460 (4)
c (Å)	5.3316 (1)	5.3681 (1)
β (°)	99.791 (2)	99.813 (2)
V (Å^3)	652.44 (1)	643.45 (2)
Calculated density (g cm^{-3})	1.478	1.406
R factors and goodness of fit	R_{wp} = 9.33%, R_p = 7.26%, χ^2 = 4.4	R_{wp} = 8.80%, R_p = 6.96%, χ^2 = 5.3

https://doi.org/10.1017/S0885715616000737 Published online by Cambridge University Press

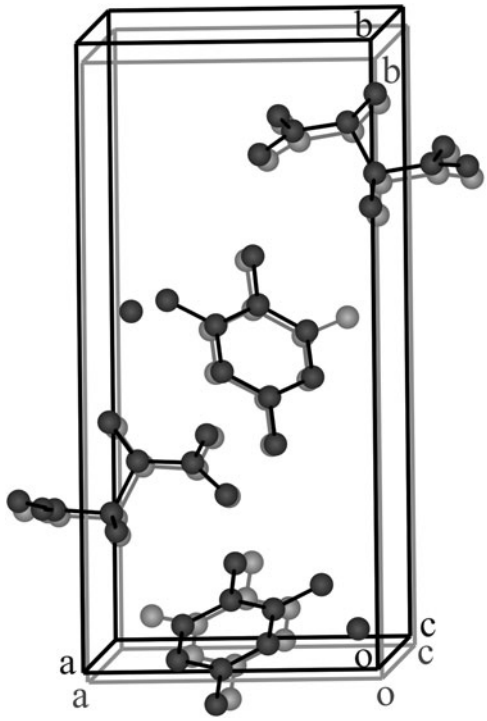

Figure 8. An overlay of the unit cells of **1** (dark gray) and **2** (light gray) viewed approximately along the *c*-axis showing different orientations of the 2,4-DAT molecules, while the TA molecules are superimposed.

Hydrogen bonding parameters for the crystal structure of **1** and **2** are given in Table IV.

E. FT-IR analysis

Proton transfer from TA to 2,4-DTA was confirmed by FT-IR analysis. According to the literature (Xu *et al.*, 2014), the carboxylic group in neutral form (–COOH) displays a characteristic absorption because of C = O stretching at around 1700 cm^{-1}. For carboxylate anion group ($–COO^{–}$), the corresponding absorption of C = O stretching shifts to a lower wavenumber. Two reasonable strong absorptions at 1712 and 1584 cm^{-1} were assigned to the C = O group from –COOH and $–COO^{–}$ groups in **1**, respectively, indicating TA is partially deprotonized. The stretching of C = O group from –COOH and $–COO^{–}$ groups in **2** appear at 1693 and 1573 cm^{-1}, respectively.

F. TGA/DSC

TGA/DSC measurements indicate a continuous water loss when heated up to 150 °C. A minor endothermic peak was observed at around 130 °C (Figure 10). Another TGA/DSC measurement was carried out at a heating rate of 5 °C min^{-1} and a significant endothermic peak was observed (figure not shown). A weight loss around 5.5% was observed at around 130 °C, corresponding 0.88 water molecule per TA/2,4-DTA adduct. A strong endothermic peak appeared in the DSC diagram together with a dramatic weight loss in the TGA curve at around 168 °C, corresponding to the decomposition of **1**.

TABLE IV. Hydrogen bonding and distances in **1** and **2**.

1		**2**	
D. . .A	Distances (Å)	D. . .A	Distances (Å)
N(23). . .O (7)	2.932 (2)	N(23). . .O(8)	3.031 (7)
N(23). . .O (8)	2.872 (3)	N(23). . .O(9)	2.756 (5)
N(23). . .O (10)	2.598 (6)	N(23). . .O(10)	2.647 (3)
O(5). . .O (9)	2.393 (4)	O(5). . .O(8)	2.433 (4)
O(5). . .N (23)	2.782 (7)	O(7). . .O(9)	2.799 (7)
O(6). . .O (10)	2.783 (6)	O(7). . .N(22)	3.033 (8)
O(6). . .O (30)	2.982 (6)		
O(7). . .O (30)	3.034 (1)		

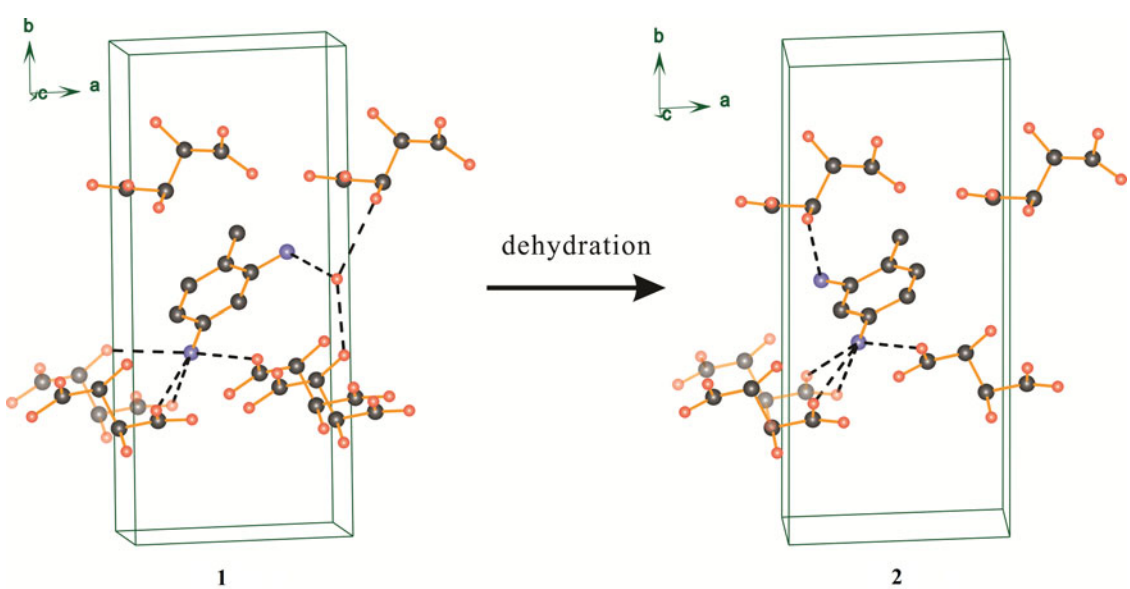

Figure 9. (Color online) Comparison of packing diagrams of the crystal structure of **1** and **2** viewed approximately along the *c*-axis. Color code is as in Figure 2. Dashed lines represent hydrogen bonds.

https://doi.org/10.1017/S0885715616000737 Published online by Cambridge University Press

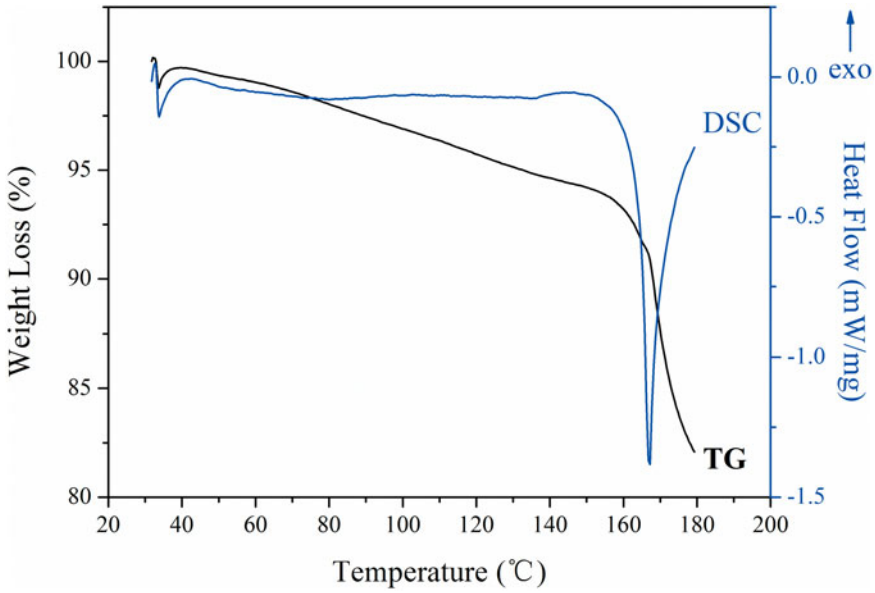

Figure 10. (Color online) TGA–DSC pattern of **1**.

IV. CONCLUSION

An organic polar hydrate based on 2,4-diaminotoluene (2,4-DAT) and L(+)-TA was crystallized and its dehydration behavior was investigated using a combination of variable temperature PXRD technique and thermal analysis. Proton transfer from L(+)-TA to 2,4-DAT was indicated by FT-IR characterization. Both hydrated and dehydrated forms crystallized in the polar space group $P2_1$. After dehydration, the L(+)-TA molecules show similar arrangements, while the 2,4-DAT molecules adopt different orientations. The finding of this work provides a way to design new organic polar materials.

ACKNOWLEDGEMENTS

We gratefully acknowledge the National Natural Science Fund for Young Scholars of China (grant no. 21107049), the Priority Academic Development Program of Jiangsu Higher Education Institutions, and the Program for Changjiang Scholars and Innovative Research Teams in Universities (grant no. IRT1146) for financial support.

SUPPLEMENTARY MATERIAL

The supplementary material for this article can be found at https://doi.org/10.1017/S0885715616000737.

Aakeroy, C. B., Cooke, T. I., and Nieuwenhuyzen, M. (**1996**). "The crystal structure of the molecular cocrystal L-malic acid L-tartaric acid (1/1)," Supramol. Chem. **7**, 153–156.

Betteridge, P. W., Carruthers, J. R., Cooper, R. I., Prout, K., and Watkin, D. J. (**2003**). "CRYSTALS version 12: software for guided crystal structure analysis," J. Appl. Crystallogr. **36**, 1487–1487.

Chen, S. and Zeng, X. C. (**2014**). "Design of ferroelectric organic molecular crystals with ultrahigh polarization," J. Am. Chem. Soc. **136**, 6428–6436.

Collet, E., Lemee-Cailleau, M. H., Buron-Le Cointe, M., Cailleau, H., Wulff, M., Luty, T., Koshihara, S. Y., Meyer, M., Toupet, L., Rabiller, P., and Techert, S. (**2003**). "Laser-induced ferroelectric structural order in an organic charge-transfer crystal," Science **300**, 612–615.

Ding, X. H., Li, Y. H., Wang, S., and Huang, W. (**2014**). "Proton-transfer supramolecular salts of D-/L-tartaric acid and 1-(2-pyrimidyl)piperazine," J. Mol. Struct. **1062**, 61–67.

Engel, G. E., Wilke, S., Konig, O., Harris, K. D. M., and Leusen, F. J. J. (**1999**). "PowderSolve – a complete package for crystal structure solution from powder diffraction patterns," J. Appl. Crystallogr. **32**, 1169–1179.

Fu, D. W., Zhang, W., Cai, H. L., Ge, J. Z., Zhang, Y., and Xiong, R. G. (**2011**). "Diisopropylammonium chloride: a ferroelectric organic salt with a high phase transition temperature and practical utilization level of spontaneous polarization," Adv. Mater. **23**, 5658–5662.

Fu, D. W., Cai, H. L., Liu, Y. M., Ye, Q., Zhang, W., Zhang, Y., Chen, X. Y., Giovannetti, G., Capone, M., Li, J. Y., and Xiong, R. G. (**2013**). "Diisopropylammonium bromide is a high-temperature molecular ferroelectric crystal," Science **339**, 425–428.

Horiuchi, S., Ishii, F., Kumai, R., Okimoto, Y., Tachibana, H., Nagaosa, N., and Tokura, Y. (**2005**). "Ferroelectricity near room temperature in co-crystals of nonpolar organic molecules," Nat. Mater. **4**, 163–166.

Hu, Z. J., Tian, M. W., Nysten, B., and Jonas, A. M. (**2009**). "Regular arrays of highly ordered ferroelectric polymer nanostructures for non-volatile low-voltage memories," Nat. Mater. **8**, 62–67.

Katrusiak, A. and Szafranski, M. (**1999**). "Ferroelectricity in NH center dot center dot center dot N hydrogen bonded crystals," Phys. Rev. Lett. **82**, 576–579.

Larson, A. C. and Von Dreele, R. B. (**2000**). *General Structure Analysis System (GSAS)* (Report LAUR 86–748) (Los Alamos National Laboratory, Los Alamos, New Mexico).

Leiserowitz, L. (**1976**). "Molecular packing modes – carboxylic-acids," Acta Crystallogr. B, Struct. Sci. **32**, 775–802.

Naber, R. C. G., Tanase, C., Blom, P. W. M., Gelinck, G. H., Marsman, A. W., Touwslager, F. J., Setayesh, S., and De Leeuw, D. M. (**2005**). "High-performance solution-processed polymer ferroelectric field-effect transistors," Nat. Mater. **4**, 243–248.

Neumann, M. A. (**2003**). "X-Cell: a novel indexing algorithm for routine tasks and difficult cases," J. Appl. Crystallogr. **36**, 356–365.

Smith, G., Wermuth, U. D., and White, J. M. (**2006**). "Proton-transfer and non-transfer in compounds of quinoline and quinaldic acid with L-tartaric acid," Acta Crystallogr. C, Cryst. Struct. Commun. **62**, O694–O698.

Szafranski, M., Katrusiak, A., and McIntyre, G. J. (**2002**). "Ferroelectric order of parallel bistable hydrogen bonds," Phys. Rev. Lett. **89**.

https://doi.org/10.1017/S0885715616000737 Published online by Cambridge University Press

Timofeeva, T. V., Kuhn, G. H., Nesterov, V. V., Nesterov, V. N., Frazier, D. O., Penn, B. G., and Antipin, M. Y. (**2003**). "Cocrystal of 1,1-dicyano-2-(4-hydroxyphenyl)-ethene with L-proline and induced conformational polymorphism of 1,1-dicyano-2-(4-hydroxy-3-methoxyphenyl)-ethene," Cryst. Growth Des. **3**, 383–391.

Toby, B. H. (**2001**). "*EXPGUI*, a graphical user interface for *GSAS*," J. Appl. Crystallogr. **34**, 210–213.

Wen, Z., Li, C., Wu, D., Li, A. D., and Ming, N. B. (**2013**). "Ferroelectric-field-effect-enhanced electroresistance in metal/ferroelectric/semiconductor tunnel junctions," Nat. Mater. **12**, 617–621.

Xu, Y., Jiang, L. L., and Mei, X. F. (**2014**). "Supramolecular structures and physicochemical properties of norfloxacin salts," Acta Crystallogr. B, Struct. Sci. Cryst. Eng. Mater. **70**, 750–760.

https://doi.org/10.1017/S0885715616000737 Published online by Cambridge University Press